Transmission Optimization and Resource Allocation for Wireless Powered Dense Vehicle Area Network with Energy Recycling

Chi Jin, *Student Member, IEEE,* Fengye Hu, *Senior Member, IEEE,* Zhuang Ling, *Student Member, IEEE,* Zhi Mao, *Student Member, IEEE,* Zheng Chang, *Senior Member, IEEE,* and Cheng Li, *Senior Member, IEEE*

***Abstract*—The wireless-powered communication paradigm brings self-sustainability to the on-vehicle sensors by harvesting the energy from radiated radio frequency (RF) signals. This paper proposes a novel transmission and resource allocation strategy for the scenario where multiple wireless powered vehicle area networks (VAN) co-existed with high density. The considered multi-VAN system consists of a remote master access point (MAP), multiple on-vehicle hybrid access points (HAPs) and sensors. Unlike previous works, we consider that the sensors can recycle the radiated radio frequency energy from all the HAPs when HAPs communicate with MAP, so the dedicated signals for energy harvesting (EH) are unnecessary. The proposed strategy can achieve simultaneous wireless information and power transfer (SWIPT) without complex receiver architecture requirements. The extra EH and interference caused by the dense distribution of VANs, which are rarely explored, are fully considered. To maximize the sum throughput of all the sensors while guaranteeing the transmission from HAPs to the MAP, we jointly optimize the time allocation, system energy consumption, power allocation, and receive beamforming. Due to the non-convexity of the formulated problem, we address the sub-problems separately through the Rayleigh quotient, Frobenius norm minimization and convex optimization. Then an efficient iterative algorithm to obtain sub-optimal solutions. The simulation results and discussions illustrate the proposed scheme's effectiveness and advantages.**

***Index Terms*—Dense network, Energy harvesting, Throughput maximization, Wireless powered network.**

I. Introduction

WIRELESS power transfer (WPT) is considered one of the critical technologies to boost the development of sustainable Internet of Things (IoT) and has become a crucial component of the sixth-generation wireless communication (6G) [1], [2]. Integrated the WPT with the low-power sensing devices, the resulted wireless powered sensing network (WPSN) has its potential for environmental monitoring, health care, and intelligent cities [3]–[6], in which WPT can realize the stable power supply for wireless sensors [7]–[9]. Especially in the field of intelligent vehicles, it is expected that a large number of onboard sensors will be equipped on future vehicles to enhance intelligence. In order to eliminate the inconvenience caused by battery charging and tangled wires, WPT has gained unprecedented interest. Compared with traditional energy harvest schemes, such as solar and mechanical energy conversion, WPT is ubiquitous, sustainable and controllable [10]. In practice, vehicle area networks (VANs) are usually densely distributed, and a single VAN can be modelled as a hybrid access point (HAP) and several onboard sensors. In a multi-VAN system (e.g., vehicles on the street), sensors can harvest energy from HAPs in neighbouring VANs, while the transmissions to the HAPs suffer interference as well. We extensively reviewed related works and found that they mainly concentrate on the single network, and there are few references for the multi-network scenario. Moreover, most of them ignore either the extra energy or the interference, which is irrational. Therefore, this work is devoted to studying a proper transmission strategy for the dense VANs, which is expected to fully utilize the benefit of energy harvesting (EH) and suppress the interference.

The investigation of simultaneous wireless information and power transfer (SWIPT) plays a vital role [11]–[17]. SWIPT enables sensors to decode information and harvest energy from the same radio frequency (RF) signal through time switching (TS) and/or power splitting (PS), which effectively avoids the delay induced by the separate energy transmission process. However, a relatively complex receiver architecture is required to support TS and PS [18]. The wireless powered communication network (WPCN) in [19] is another practical network paradigm that is regarded as a particular case of SWIPT. The research on the WPCN has also received increasing interest over the past few years [20], [21]. WPCN avoids complex receiver design and adopts the time division multiple access (TDMA) based "harvest-then-transmit" (HTT) protocol, making it more attractive for on-board devices. However, WPCN does not make full use of the WEH phase.

Although there has been much research based on SWIPT or WPCN, they only consider the scenario where the network includes a single HAP. Their proposed strategies, such as relaying, PS/TS optimization, and energy allocation, are unsuitable for the multi-network scenario, where the received

(*Corresponding author: Fengye Hu)*

C. Jin, F. Hu, Z. Ling and Z. Mao are with the College of Communication Engineering, Jilin University, Changchun, China (Email: jinchi19@mails.jlu.edu.cn, hufy@jlu.edu.cn, lingzhuang@jlu.edu.cn, zhimao17@mails.jlu.edu.cn).

Z. Chang is with Faculty of Information Technology, University of Jyväskylä, FIN-40014 Jyväskylä, Finland (Email: zheng.chang@jyu.fi).

C. Li is with Faculty of Engineering and Applied Science, Memorial University, St. John's, NL, A1B 3X5, Canada (Email: licheng@mun.ca).

This work was supported by Joint Fund for Regional Innovation and Development of the National Natural Science Foundation of China (No.U21A20445) and National Natural Science Foundation of China (No.61671219).

signal is more complicated at both the HAP and the sensors. Particularly, in [22] the EH is optimized only for a single user with the consideration of the Rician fading channel. In [23], the authors maximize the weighted sum throughput for a similar system. Then, in [24], the minimum throughput among different sensors in a single network is maximized for fairness.In [25], the authors design a transmission security scheme for a single-AP multi-user. In [26], the power consumption is minimized to achieve maximum energy efficiency. In [27], the user pairing scheme is considered, where users close to the source harvest energy with the PS or TS strategy and act as relays for remote users.

Some joint optimization methods can provide reference for the optimization of multi-network system. In [28], a joint optimization scheme with uplink and downlink beamforming is investigated to make full use of multiple antennas. The authors of [29] improve the energy efficiency by jointly optimizing the beamforming, transmission power, and PS ratio. Combined with lightweight artificial intelligence (AI) technology, the authors realize dynamic management and power control during the energy harvesting process in [30]. The author of [31] proposes an intra-group cooperative strategy that converts the multiple input single output (MISO) system into a multiple input multiple output (MIMO) system through the cooperation of single-antenna users and realizes the transmit beamforming at the sensor side.

All the strategies above are only devised for a single VAN with one HAP. To date, only a few practical works have been done for the multi-AP network [32]–[37]. Either extra harvested energy or adjacent interference is ignored in most related studies. The authors of [33] design the power allocation and wireless backhaul bandwidth allocation strategy in heterogeneous small cell networks but assume the sensors have sufficient power. Under similar assumption, wireless resource allocation is carried out for APs with overlapping coverage to save power in [34]. A cooperative transmission scheme for clustered wireless sensor networks is studied in [35], but the interference is not considered. The authors in [36], [37] investigate the energy gain and interference cancellation in the multi-AP scenarios, with the consideration that each HAP can serve only one user.

Bearing in mind the features of a multi-VAN system, we focus on the development of multi-AP WPSN. In the system, the HAP can deliver wireless power to the sensors and receive data from them. It is noteworthy that due to the insufficient computing resources, HAPs in the considered scenario upload data to the remote master access point (MAP) for fusion, computing, or other functions. Such uplink transmission can be carried out in the downlink WEH phase. Meanwhile, sensors can also recycle the RF signals for EH instead of the dedicated energy signal. This transmission protocol integrates the advantages of WPCN and SWIPT, and is more suitable for a multi-VAN system with low-power devices. The main contributions of this paper can be summarized as follows:

- A multi-VAN system is considered. The extra EH and interference caused by adjacent networks, which have been rarely studied, are thoroughly considered when optimizing the system performance. A TDMA-based transmission protocol that enables the HAPs to power up sensors while communicating with the remote MAP is designed. A transmission strategy is proposed to optimize the system energy consumption (E), time segment factor (τ), transmission power ($\boldsymbol{P}_{Ap}$), energy allocation weights ($\boldsymbol{W}$), and receive beamforming ($\boldsymbol{B}$).
- In order to maximize the system throughput, $\{E, \tau, \boldsymbol{P}_{Ap}, \boldsymbol{W}, \boldsymbol{B}\}$ are optimized separately at first. The objective function is monotonic about E and τ but non-convex on $\boldsymbol{B}$ and $\boldsymbol{W}$. Various constraints are considered explicitly, and $\boldsymbol{W}$ is jointly shared by all sensors, so the optimization problem is challenging to solve. The Rayleigh quotient, Frobenius norm minimization, convex optimization and an efficient alternating approach are adopted for investigating the optimal transmission strategy π^*.
- A high-quality sub-optimal solution is obtained through the proposed algorithm. Extensive simulations are conducted, and some crucial characteristics observed in the simulation results are illustrated. Moreover, we further investigate the effect of each variable under different constraints, of which some key findings on the transmission strategy design are concluded.

The rest of this paper is organized as follows. The system model is introduced in Section II. The optimization problem is formulated, and the strategy is discussed in Section III. Numerical results and insights are presented in Section IV. Finally, Section V concludes the work.

TABLE I
LIST OF NOTATIONS

Symbol	Definition
AP_i	The HAP in the ith VAN
S_{ij}	The jth sensor in the ith VAN
$\hat{S}_{i,t}$	The sensor that transmit at slot t in the ith VAN
N_V	Total number of VANs/HAPs
M_i	Total number of sensors in the ith VAN
$\hat{x}^i_{Ap}$	Transmitted signal of AP_i
$\hat{x}^{ij}_{S}$	Transmitted signal of S_{ij}
y^i_{Ap}	Received signal of AP_i
y^{ij}_{S}	Received signal of S_{ij}
$\boldsymbol{H}^{ij}_k$	Channel from AP_k to S_{ij}
$\boldsymbol{G}^k_{ij}$	Channel from S_{ij} to AP_k
$\boldsymbol{U}_i$	Channel from AP_i to MAP
$\boldsymbol{V}_i$	MRT weight for signals from AP_i to MAP
P^i_{Ap}	Transmission power of AP_i
P^{ij}_{S}	Transmission power of S_{ij}
τ	Time segment factor
E	Rated energy consumption per time block
$\boldsymbol{W}$	Power allocation weights for HAPs
$\boldsymbol{B}_{it}$	Receive beamforming for signals from $\hat{S}_{i,t}$ to AP_i

II. System Model

As shown in Fig. 1, we consider a multi-VAN system with N_V VANs and a distant MAP. Each VAN contains a single HAP denoted by AP_i ($i = 1, 2, \cdots, N_V$) and M_i wirelessly powered sensors denoted by S_{ij} ($j = 1, 2, \cdots, M_i$). It is assumed that the vehicles are densely distributed, and the distances between HAPs and MAP are much farther than

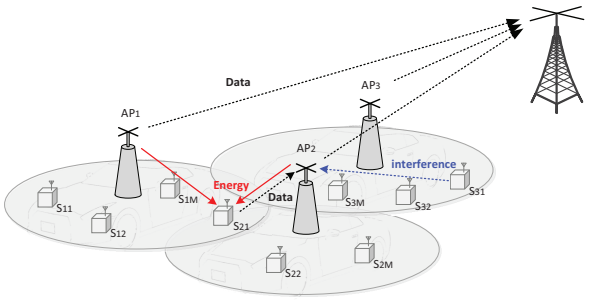

Fig. 1. Wireless powered multi-VAN overlapping system.

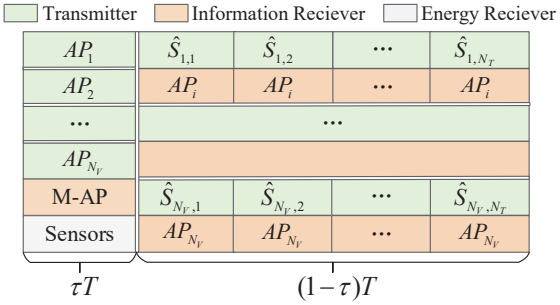

Fig. 2. Transmission scheme.

the distance among HAPs. The HAPs gather the perception data from sensors and forward the data in the following transmission block to the MAP. The MAP is responsible for data fusion, decision, and control functions. The RF energy radiated during the communication phase between HAP and MAP is recycled by the sensors. The HAPs and MAP are equipped with A and $A_M(\geq N_V)$ antennas and sufficient energy resources. Each sensor has a single antenna and performs the transmission with the harvested energy. All devices operate in half-duplex mode.

The channels from HAPs to MAP and sensors are independent of each other. It is assumed that the channels are quasi-static fading, where channel status remains constant during each transmission time block but varies from one block to another. It is further assumed that the HAPs and MAP know channel status perfectly at the beginning of each block.

As shown in Fig. 2, a FTDMA-based transmission scheme is presented. We set the time block length as T and the time segment factor as τ. Each time block is divided into two phases: the wireless EH (WEH) phase and the wireless information transmission (WIT) phase. HAPs transmit information (such as the perception data uploaded by sensors) to MAP simultaneously with different carrier frequencies. Sensors can recycle the radiated RF energy from HAPs. The recycled energy is stored in a supercapacitor for the following data transmission. In the WIT phase, time is divided equally into $N_T(\geq M_i)$ slots and each slots has the length of $(1-\tau)T/N_T$. It should be aware that a sensor may be assigned with multiple time slots rather than only a single. The carrier frequencies of sensors uploading data in the same time slot may be the same, partially the same, or completely different.

A. WEH Phase

The system energy consumption per time block is denoted as E, and $\boldsymbol{W} = [w_1, \cdots, w_{N_V}]$ is the energy allocation weight vector for HAPs (i.e., $\boldsymbol{W}\boldsymbol{W}^H = 1$). Thus, the transmission energy assigned for AP_i is $w_i^2 E$, and the total transmission power of AP_i is given by

$$P_{Ap}^i = \frac{w_i^2 E}{\tau T} = w_i^2 P, \tag{1}$$

where we define $P = E/(\tau T)$. P_{max} is the maximum transmission power for HAPs, so $P_{Ap}^i \leq P_{max}$ is necessary.

Suppose MAP allocates only a single receiving antenna per HAP, and the channel from AP_i to MAP can be expressed as

$$\boldsymbol{U}_i = \left[\ u_{i1}, u_{i2}, \ldots, u_{iA}\ \right]^H. \tag{2}$$

For element u_{iA}, the subscript iA indicates the source (AP_i's Ath antenna). In order to improve the throughput performance, the maximal ratio transmission (MRT) method is adopted at the HAP side. MRT is a widely used antenna diversity technology that enables the receiver to achieve the highest signal-to-noise ratio and effectively resist multipath fading [38], [39]. According to MRT, the transmission weight vector for the A antennas of AP_i can be obtained by $\boldsymbol{V}_i = \boldsymbol{U}_i/|\boldsymbol{U}_i| = [v_{i1}, v_{i2}, \cdots, v_{iA}]^H$. Furthermore, we have $\boldsymbol{V} = [\boldsymbol{V}_1, \boldsymbol{V}_2, \cdots, \boldsymbol{V}_{N_V}]^H$, and the transmitted signal is

$$\hat{\boldsymbol{x}}_{Ap}^i = \boldsymbol{V}_i^H \sqrt{P_{Ap}^i} x_{Ap}^i = \boldsymbol{V}_i^H \sqrt{P} w_i x_{Ap}^i. \tag{3}$$

x_{Ap}^i is the normalized information signal, i.e., $E[|x_{Ap}^i|^2] = 1$, where $E[\cdot]$ stands for the expectation operator.

The signal received from AP_i can be expressed as:

$$y_M(i) = \boldsymbol{V}_i^H \boldsymbol{U}_i \sqrt{P} w_i x_{Ap}^i + n_M^i, \tag{4}$$

where $n_M^i \sim \mathcal{CN}(0, \sigma_M^2)$ represents the additive white Gaussian noise at the antenna of MAP. The signal to noise ratio (SNR) for signal from AP_i is expressed as

$$\Gamma_i = \frac{P w_i^2 |\boldsymbol{V}_i^H \boldsymbol{U}_i|^2}{\sigma_M^2}. \tag{5}$$

Assuming that the uplink transmission bandwidth of AP_i is ℓ_i, the throughput from AP_i to MAP can be given by

$$r_i = \ell_i \tau T log_2 \left(1 + \frac{P w_i^2 |\boldsymbol{V}_i^H \boldsymbol{U}_i|^2}{\sigma_M^2}\right). \tag{6}$$

Given that Υ_i is the minimum throughput requirement for AP_i to communicate with MAP, then $r_i > \Upsilon_i$ should be satisfied, and we have

$$w_i \geq \sqrt{\left(2^{\frac{\Upsilon_i}{\ell_i \tau T}} - 1\right) \frac{\sigma_M^2}{P |\boldsymbol{V}_i^H \boldsymbol{U}_i|^2}} = w_i^{lb}, \tag{7}$$

where w_i^{lb} is the lower bound of w_i. Substituting $P = E/\tau T$ into (6) and solving $r_i > \Upsilon_i$, we get

$$E \geq \left(2^{\frac{\Upsilon_i}{\ell_i \tau T}} - 1\right) \frac{\tau T \sigma_M^2}{w_i^2 |\boldsymbol{V}_i^H \boldsymbol{U}_i|^2} = E_i^{lb}, \tag{8}$$

$$\tau \geq -\frac{F ln(J)}{F\Omega(-\frac{J^{-1/F} ln(J)}{F}) + ln(J)} = \tau_i^{lb}, \tag{9}$$

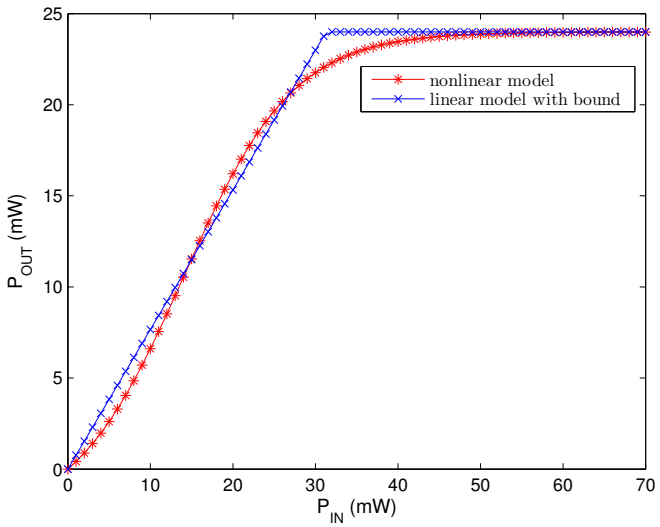

Fig. 3. Comparison on linear and nonlinear EH model.

$$\ell_i \geq \Upsilon_i \left[\tau T log_2 \left(1 + \frac{E w_i^2 |\boldsymbol{V}_i^H \boldsymbol{U}_i|^2}{\tau T \sigma_M^2} \right) \right]^{-1} = \ell_i^{lb} \tag{10}$$

where ℓ_i^{lb}, τ_i^{lb} and E_i^{lb} are the lower bounds of ℓ_i, τ and E. The operator $\Omega(\cdot)$ represents the product log function, and $F = E w_i^2 |\boldsymbol{V}_i^H \boldsymbol{U}_i|^2 / (T\sigma_M^2)$, $J = 2^{\Upsilon_i / T\ell_i}$.

Next, we analyze the EH process on the sensor side. The channel from AP_k ($k = 1, \cdots, N$) to S_{ij} is denoted as $\boldsymbol{H}_k^{ij} = [h_{k1}^{ij}, h_{k2}^{ij}, \cdots, h_{kA}^{ij}]^H$. For element h_{kA}^{ij}, the subscript kA indicates the source (AP_k's Ath antenna) and the superscript ij indicates the destination (S_{ij}'s single antenna). At slot k, the received signal at S_{ij} can be expressed as

$$\begin{aligned} y_S^{ij}(k) &= \sum_{k=1}^{N_V} \sum_{a=1}^{A} h_{ka}^{ij} v_{ka} \sqrt{P} w_k x_{Ap}^k + n_S \\ &= \sum_{k=1}^{N_V} \sum_{a=1}^{A} \hat{h}_{ka}^{ij} \sqrt{P} w_k x_{Ap}^k + n_S \end{aligned} \tag{11}$$

where $n_S \sim \mathcal{CN}(0, \sigma_S^2)$ represents the additive white Gaussian noise at the antenna of sensors.

The linear and non-linear energy harvest models are proved to be approximately equivalent in low power scenarios [40]. The comparison curves are shown in Fig. 3. We denote the EH model as a linear function: $P_{harvest} = \eta P_{receive}$, η $(0 < \eta < 1)$ is the energy conversion ratio. The total energy harvested by S_{ij} during the WEH phase can be expressed as

$$E_S^{ij} = \eta\tau T \left(P \left| \boldsymbol{W} \hat{\boldsymbol{H}}_{ij} \right|^2 + \sigma_S^2 \right) \approx \eta\tau T P \left| \boldsymbol{W} \hat{\boldsymbol{H}}_{ij} \right|^2 \tag{12}$$

Here item $\eta\tau T\sigma_S^2$ is ignored since it is rather smaller than the front one in practice [41]. $\hat{\boldsymbol{H}}_{ij} = \boldsymbol{H}_{ij} \odot \boldsymbol{V}$ and the operator $\odot$ represents the Hadamard product.

B. WIT Phase

In the WIT phase, sensors transmit information by using the energy harvested in the WEH phase. Let $\hat{\mu}_i = [\mu_{i1}, \mu_{i2}, \cdots, \mu_{iM_i}]$ denote the numbers of time slots assigned for sensors in subnet i, then the transmission power of S_{ij} can be written as

$$P_S^{ij} = \frac{E_S^{ij}}{\mu_{ij}(1-\tau)T/N_T} = \frac{\eta\tau N_T P \left| \boldsymbol{W} \hat{\boldsymbol{H}}_{ij} \right|^2}{\mu_{ij}(1-\tau)}. \tag{13}$$

The signal transmitted at S_{ij} is

$$\hat{x}_S^{ij} = \sqrt{P_S^{ij}} x_S^{ij}, \tag{14}$$

where x_S^{ij} is the normalized information signal, i.e., $E[|x_S^{ij}|^2] = 1$. The channel from S_{kj} to AP_i is denoted by $\boldsymbol{G}_{kj}^i = [g_{kj}^{i1}, g_{kj}^{i2}, \cdots, g_{kj}^{iA}]^H$, where the subscript indicates the source (S_{kj}) and the superscript iA indicates the destination (AP_i's Ath antenna).

To simplify the description, we use $\hat{S}_{i,t}$ to indicate the sensor that uploads data in subnet i during slot t. Due to the coexistence of multiple subnets, AP_i receives not only the information signal from $\hat{S}_{i,t}$ at slot t, but also the interference signal from $\hat{S}_{k,t}$ ($k \neq i$). To improve the SNR, and $\boldsymbol{B}_{it} = [b_{it}^1, b_{it}^2, \cdots, b_{it}^A]$ is designed as the receive weight vector for AP_i at slot t. Therefore, the received signal of AP_i can be given by

$$y_{Ap}^i(t) = \boldsymbol{B}_{it} \left[\sum_{j=1}^{M_k} \sum_{k=1}^{N_V} \hat{\iota}_{kj,t} \hat{\kappa}_{kj,t}^i \boldsymbol{G}_{kj}^i \sqrt{P_S^{kj}} x_S^{kj} + \boldsymbol{n}_{Ap} \right]. \tag{15}$$

where $\boldsymbol{n}_{Ap} = [n_{Ap}^1, n_{Ap}^2, \cdots, n_{Ap}^A]^H$ represents the additive white Gaussian noise at antennas of HAP and $n_{Ap}^a \sim \mathcal{CN}(0, \sigma_{Ap}^2)$. $\hat{\iota}_{kj,t}$ is the indication for time slot allocation, $\hat{\iota}_{kj,t} = 1$ if sensor S_{kj} transmits in time slot t (that is, S_{kj} can be be denoted as $\hat{S}_{k,t}$), otherwise it is 0. $\hat{\kappa}_{kj,t}^i$ is the interference factor. If S_{kj} uploads data with the same carrier frequency as $\hat{S}_{i,t}$, then $\hat{\kappa}_{kj,t}^i = 1$, otherwise it is 0. When AP_i receives information signal from $\hat{S}_{i,t}$, the SNR is expressed as

$$\gamma_{it} = \frac{\sum_{j=1}^{M_i} \hat{\iota}_{ij,t} \hat{\kappa}_{ij,t}^i P_S^{ij} \left| \boldsymbol{B}_{it} \boldsymbol{G}_{ij}^i \right|^2}{\sum_{j=1}^{M_k} \sum_{k=1, k\neq i}^{N_V} \hat{\iota}_{kj,t} \hat{\kappa}_{kj,t}^i P_S^{kj} \left| \boldsymbol{B}_{it} \boldsymbol{G}_{kj}^i \right|^2 + |\boldsymbol{B}_{it}|^2 \sigma_{Ap}^2}. \tag{16}$$

We define $\boldsymbol{B}_i = [\boldsymbol{B}_{i1}^H, \boldsymbol{B}_{i2}^H, \cdots, \boldsymbol{B}_{iN_T}^H]$, and all $\boldsymbol{B}_i$s determine the tensor $\boldsymbol{B}$.

It is assuming that the uplink bandwidth of the sensor is ℓ_S, which is equally divided into N_{SF} frequency bands for multiplexing. The co-channel interference can be avoided by scheduling if $N_{SF} \geq Min(N_T, N_V)$, or it will inevitably occur in some time slots or subnets. The operator $Min(\cdot)$ means to take the minimum value. The sum throughput from sensors to HAP in the ith VAN can be expressed as

$$C_i(\boldsymbol{W}, \boldsymbol{B}_i, E, \tau) = \hat{\ell}_S \sum_{t=1}^{N_T} \frac{(1-\tau)T}{N_T} log_2(1 + \gamma_{it}). \tag{17}$$

where $\hat{\ell}_S = (\ell_S - \ell_{\Delta S})/N_{SF}$, $\ell_{\Delta S}$ is the reserved bandwidth, which can be used as frequency band gaps to avoid aliasing.

III. Problem Formulation and Optimization Strategy

In this section, we first present the formulated problem and investigate the optimization strategy. As one can see from (17), the optimization variables are system energy consumption E, time segment factor τ, transmission power $\boldsymbol{P}_{Ap}$, energy allocation weights $\boldsymbol{W}$, and receive beamforming $\boldsymbol{B}$. The overall problem is formulated to maximize the sum-throughput of sensors while guaranteeing the communication between HAPs and MAP:

$$\begin{aligned}(P1): \quad & \max_{\boldsymbol{W},\boldsymbol{B},E,\tau} \sum_{i=1}^{N_V} C_i(\boldsymbol{W},\boldsymbol{B}_i,E,\tau) \\ & C1: \boldsymbol{W} \succeq \boldsymbol{W}^{lb}, \\ & C2: \boldsymbol{W}\boldsymbol{W}^H = 1, \\ s.t. \quad & C3: \boldsymbol{B}_{it} \preceq \boldsymbol{1}_{1\times N}, \\ & C4: \tau^{lb} \le \tau < 1, \\ & C5: P_{Ap}^i \le P_{max},\end{aligned} \tag{18}$$

where $C1$ guarantees successful communication from the HAPs to the MAP. $\boldsymbol{W}^{lb} = [w_1^{lb}, w_2^{lb}, \cdots, w_{N_V}^{lb}]$ is given in (7) as the lower bound of $\boldsymbol{W}$. $C2$ limits the energy consumption per time block as E. It is simplified from $(\sum_{i=1}^{N} w_i^2 P)\tau T = E$ and indirectly bounds that $w_i < 1$. $C3$ means the receive weights must be less than 1 since the antennas cannot amplify the received signals. $C4$ denotes the lower and upper bound of time segment factors. τ^{lb} equals $Max(\tau_i^{lb})$ since τ should be greater than all τ_i^{lb}s as mentioned in (9). Here $Max(\cdot)$ means to take the maximum value. $C5$ indicates that the transmission power of HAPs cannot exceed the maximum transmission power. In order to address the formulated problem, we devide it into several sub-problems and present the corresponding solutions.

A. Receive beamforming optimization

We first optimize $\boldsymbol{B}$ and fix variables $\boldsymbol{W}$, E and τ as constants. We define $\boldsymbol{D}_{it}^n(\boldsymbol{W},E,\tau) = \sum_{j=1}^{M_k}\sum_{k=1}^{N_V} \hat{\iota}_{kj,t}\hat{\kappa}_{kj,t}^i N_T\eta E|\boldsymbol{W}\hat{\boldsymbol{H}}_{kj}|^2|\boldsymbol{G}_{kj}^i|^2/\mu_{kj} + (1-\tau)T\sigma_{Ap}^2\boldsymbol{I}_A$, $\boldsymbol{D}_{it}^d(\boldsymbol{W},E,\tau) = \sum_{j=1}^{M_k}\sum_{k=1,k\neq i}^{N_V} \hat{\iota}_{kj,t}\hat{\kappa}_{kj,t}^i N_T\eta E|\boldsymbol{W}\hat{\boldsymbol{H}}_{kj}|^2|\boldsymbol{G}_{kj}^i|^2/\mu_{kj} + (1-\tau)T\sigma_{Ap}^2\boldsymbol{I}_A$, where $\boldsymbol{I}_A$ is the A-order identity matrix, then the sum-throughput can be written as

$$C(\boldsymbol{B}) = \hat{\ell}_S\hat{\tau}\sum_{i=1}^{N_V}\sum_{t=1}^{N_T} log_2\left(\frac{\boldsymbol{B}_{it}\boldsymbol{D}_{it}^n(\boldsymbol{W},E,\tau)\boldsymbol{B}_{it}^H}{\boldsymbol{B}_{it}\boldsymbol{D}_{it}^d(\boldsymbol{W},E,\tau)\boldsymbol{B}_{it}^H}\right), \tag{19}$$

which is the sum of $N_V \times N_T$ logarithmic functions. Here $\hat{\tau} = (1-\tau)T/N_T$. $\boldsymbol{B}$ can be achieved by optimizing $\boldsymbol{B}_{it}$ separately since $\boldsymbol{B}_{it}$s are independent. Considering the monotonicity of logarithmic function, $(P1)$ can be transformed into $N_V \times N_T$ optimization problems as

$$\begin{aligned}(P2): \quad & \max_{\boldsymbol{B}_{it}} \frac{\boldsymbol{B}_{it}\boldsymbol{D}_{it}^n(\boldsymbol{W},E,\tau)\boldsymbol{B}_{it}^H}{\boldsymbol{B}_{it}\boldsymbol{D}_{it}^d(\boldsymbol{W},E,\tau)\boldsymbol{B}_{it}^H} \\ s.t. \quad & \boldsymbol{B}_{it} \preceq \boldsymbol{1}_{1\times N}.\end{aligned} \tag{20}$$

According to generalized Rayleigh quotient theory, the optimal solution $\boldsymbol{B}_{it}^*$ can be solved by calculating the normalized eigenvector corresponding to the largest eigenvalue of matrix $\boldsymbol{D}_{it} = (\boldsymbol{D}_{it}^d)^{-1}\boldsymbol{D}_{it}^n$. We define this operator as $Eigmaxv$, thus

$$\boldsymbol{B}_{it}^* = Eigmaxv(\boldsymbol{D}_{it}). \tag{21}$$

B. Energy allocation optimization

Analogously, variables $\boldsymbol{B}$, E and τ are fixed to solve $\boldsymbol{W}$. We define that $\boldsymbol{Q}_{it}^n(\boldsymbol{B}_{it},E,\tau) = \sum_{j=1}^{M_k}\sum_{k=1}^{N_V} \hat{\iota}_{kj,t}\hat{\kappa}_{kj,t}^i N_T E\eta \left|\boldsymbol{B}_{it}\boldsymbol{G}_{kj}^i\right|^2 \left|\hat{\boldsymbol{H}}_{kj}\right|^2/\mu_{kj} + (1-\tau)T\left|\boldsymbol{B}_{it}\right|^2\sigma_{Ap}^2\boldsymbol{I}_{N_V}$, $\boldsymbol{Q}_{it}^d(\boldsymbol{B}_{it},E,\tau) = \sum_{j=1}^{M_k}\sum_{k=1,k\neq i}^{N_V} \hat{\iota}_{kj,t}\hat{\kappa}_{kj,t}^i N_T E\eta \left|\boldsymbol{B}_{it}\boldsymbol{G}_{kj}^i\right|^2 |\hat{\boldsymbol{H}}_{kj}|^2/\mu_{kj} + (1-\tau)T|\boldsymbol{B}_{it}|^2\sigma_{Ap}^2\boldsymbol{I}_{N_V}$. The optimization problem is given by

$$\begin{aligned}(P3): \max_{\boldsymbol{W}} \ & \hat{\ell}_S\hat{\tau}\sum_{i=1}^{N_V}\sum_{t=1}^{N_T} log_2\left(\frac{\boldsymbol{W}\boldsymbol{Q}_{it}^n(\boldsymbol{B}_{it},E,\tau)\boldsymbol{W}^H}{\boldsymbol{W}\boldsymbol{Q}_{it}^d(\boldsymbol{B}_{it},E,\tau)\boldsymbol{W}^H}\right) \\ & C1: \boldsymbol{W} \succeq \boldsymbol{W}^{lb}, \\ s.t. \quad & C2: \boldsymbol{W}\boldsymbol{W}^H = 1, \\ & C3: \boldsymbol{W} \preceq \boldsymbol{W}^{ub}.\end{aligned} \tag{22}$$

Here $C3$ is inferred from constraint $P_{Ap}^i \le P_{max}$ and we have $\boldsymbol{W}^{ub} = [w_1^{ub}, w_2^{ub}, \cdots, w_{N_V}^{ub}] = \left(\sqrt{P_{max}\tau T/E}\right)_{1\times N_V}$. The objective function is similar to (19), but $\boldsymbol{W}$ is shared by $\sum_{i=1}^{N_V} M_i$ addends unitedly. A global optimization method based on vector similarity is proposed to extract the globally optimal $\boldsymbol{W}^*$ from the individually optimal $\boldsymbol{W}_{it}^*$s. We introduce $\boldsymbol{W}_{it} = [w_{it}^1, w_{it}^1, \cdots, w_{it}^{N_V}]$ for $\hat{S}_{i,t}$ and divide $(P3)$ into $N_V \times N_T$ optimization problems. The optimal weights for $\hat{S}_{i,t}$ (i.e., $\boldsymbol{W}_{it}^*$) can be solved by Rayleigh quotient theory. Then Frobenius norm is adopted to solve $\boldsymbol{W}^*$. In the following, individual and global optimization methods are discussed respectively.

1) Optimization for individual sensor: In the individual optimization, we transform the optimization problem into Rayleigh quotient maximization as

$$\begin{aligned}(P4): \quad & \max_{\boldsymbol{W}_{it}} \frac{\boldsymbol{W}_{it}\boldsymbol{Q}_{it}^n(\boldsymbol{B}_{it},E,\tau)\boldsymbol{W}_{it}^H}{\boldsymbol{W}_{it}\boldsymbol{Q}_{it}^d(\boldsymbol{B}_{it},E,\tau)\boldsymbol{W}_{it}^H} \\ & C1: \boldsymbol{W}_{it} \succeq \boldsymbol{W}^{lb}, \\ s.t. \quad & C2: \boldsymbol{W}_{it}\boldsymbol{W}_{it}^H = 1, \\ & C3: \boldsymbol{W}_{it} \preceq \boldsymbol{W}^{ub}.\end{aligned} \tag{23}$$

Theorem 1: Define $\mathcal{A}_{it}^{ml}$ as the element in row m, column l $(m,l = 1,\ldots,N_V)$ of $\mathcal{A}_{it}$, $\vartheta_l = \sum_{m=1,m\neq l}^{N_V}\mathcal{A}_{it}^{ml}(k_{it}^m)^*$, and $\boldsymbol{Q}_{it} = (\boldsymbol{Q}_{it}^d(\boldsymbol{B}_{it},E,\tau))^{-1}\boldsymbol{Q}_{it}^n(\boldsymbol{B}_{it},E,\tau)$. The solution of $(P4)$ can be written as $\boldsymbol{W}_{it}^* = \boldsymbol{K}_{it}^*(\boldsymbol{Q}_{it}^d(\boldsymbol{B}_{it},E,\tau))^{-1/2}$, where $\boldsymbol{K}_{it}^* = [(k_{it}^1)^*, (k_{it}^2)^*, \cdots, (k_{it}^{N_V})^*]$ is given by

$$(k_{it}^l)^* = \begin{cases} (k_{it}^l)^{ub} & \tilde{w}_{it}^l > w_l^{ub}. \\ \dfrac{\vartheta_l}{\hat{\beta} - \mathcal{A}_{it}^{ll}} & w_l^{lb} \le \tilde{w}_{it}^l \le w_l^{ub}, \\ (k_{it}^l)^{lb} & \tilde{w}_{it}^l < w_l^{lb}. \end{cases} \tag{24}$$

Here $\mathcal{A}_{it} = \boldsymbol{Q}_{it} \odot \mathcal{P}_{it}^1 \odot \cdots \odot \mathcal{P}_{it}^{N_V}$, and $\hat{\beta}$ ensures $\boldsymbol{W}_{it}^*(\boldsymbol{W}_{it}^*)^H = 1$. The operator $\odot$ represents the Hadamard product. $\boldsymbol{K}_{it}^{lb} = [(k_{it}^1)^{lb}, (k_{it}^2)^{lb}, \cdots, (k_{it}^{N_V})^{lb}]$ is defined as

Algorithm 1 Individual optimal solution

Input: $\boldsymbol{Q}_{it}(\boldsymbol{B}_{it}, E, \tau)$. $i = 1, \ldots, N_V$, $t = 1, \ldots, N_T$;
Output: $\boldsymbol{W}_{it}^*$;
for $i = 1$ to N_V, **do**
  for $t = 1$ to N_T, **do**
    Compute $\tilde{\boldsymbol{W}}_{it}$ with (25);
    for $l = 1$ to N_V, **do**
      if $\tilde{w}_{it}^l < w_l^{lb}$ or $\tilde{w}_{it}^l > w_l^{ub}$
        Set $\varsigma_{it}^l = (k_{it}^l)^{lb}$ or $(k_{it}^l)^{ub}$, $z_{it}^l = 0$, compute $\mathcal{P}_{it}^l$, and update $\mathcal{A}_{it}$;
      else
        Set $\varsigma_{it}^l = 0$, $z_{it}^l = 1$;
      end if
    end for
    Compute $\mathcal{E}_{it} = Eigmaxv(\mathcal{A}_{it})$, and set $\hat{\boldsymbol{Z}}_{it} = \boldsymbol{Z}_{it} \odot \mathcal{E}_{it}$;
    Scale $\hat{\boldsymbol{Z}}_{it}$ with $|\hat{\boldsymbol{Z}}_{it}|^2 + |\mathcal{S}_{it}|^2 = 1$, and set $\boldsymbol{K}_{it}^* = \hat{\boldsymbol{Z}}_{it} + \mathcal{S}_{it}$;
    Compute $\boldsymbol{W}_{it}^* = \boldsymbol{K}_{it}^*(\boldsymbol{Q}_{it}^d(\boldsymbol{B}_{it}, E, \tau))^{-1/2}$;
  end for
end for

$\boldsymbol{W}^{lb}(\boldsymbol{Q}_{it}^d)^{1/2}$, $\boldsymbol{K}_{it}^{ub} = \boldsymbol{W}^{ub}(\boldsymbol{Q}_{it}^d)^{1/2}$. We define $\tilde{\boldsymbol{W}}_{it} = [\tilde{w}_{it}^1, \tilde{w}_{it}^2, \cdots, \tilde{w}_{it}^{N_V}]$ as

$$\tilde{\boldsymbol{W}}_{it} = \frac{Eigmaxv(\boldsymbol{Q}_{it})(\boldsymbol{Q}_{ii}^d)^{-1/2}}{|Eigmaxv(\boldsymbol{Q}_{it})(\boldsymbol{Q}_{it}^d)^{-1/2}|^2}. \tag{25}$$

$\mathcal{P}_{it}^l$ is an all-one matrix when $\tilde{\boldsymbol{W}}_{it} \succeq \boldsymbol{W}^{lb}$. If there is $\tilde{w}_{it}^l < w_l^{lb}$ ($\tilde{w}_{it}^l > w_l^{ub}$), $\mathcal{P}_{it}^l$ multiplies its lth row by $k_l/(k_{it}^l)^{ub}$ (or $k_l/(k_{it}^l)^{lb}$) and the lth column by $(k_{it}^l)^{ub}/k_l$ (or $(k_{it}^l)^{lb}/k_l$).

Proof. Please see Appendix A. □

Algorithm 1 solves $\boldsymbol{W}_{it}^*$ according to Theorem 1. $\boldsymbol{K}_{it}$, $\boldsymbol{Z}_{it}$, $\hat{\boldsymbol{Z}}_{it}$ and $\mathcal{S}_{it}$ are $1 \times N$ auxiliary vectors composed of elements k_{it}^l, z_{it}^l, $\hat{z}_{it}^l$ and ς_{it}^l. Algorithm 1 can be summarized as: First, calculate the eigenvector corresponding to the largest eigenvalue of the matrix $\boldsymbol{Q}_{it}$. Second, compute $\tilde{\boldsymbol{W}}_{it}$ with (25) and compare with $\boldsymbol{W}^{lb}$ and $\boldsymbol{W}^{ub}$. Next, fix the corresponding element in $\boldsymbol{K}_{it}$ (i.e., k_{it}^l) as $(k_{it}^l)^{lb}$ if $\tilde{w}_{it}^l < w_l^{lb}$ or $(k_{it}^l)^{ub}$ if $\tilde{w}_{it}^l > w_l^{ub}$. Then, calculate $\mathcal{P}_{it}^l$ and get the modified matrix $\mathcal{A}_{it}$. Besides, keep the aforementioned fixed elements unchanged, scale $Eigmaxv(\mathcal{A}_{it})$ partially with $|Eigmaxv(\mathcal{A}_{it})| = 1$, and denote the result as $\boldsymbol{K}_{it}^*$. Finally, calculate $\boldsymbol{W}_{it}^*$ with $\boldsymbol{W}_{it}^* = \boldsymbol{K}_{it}^*(\boldsymbol{Q}_{it}^d(\boldsymbol{B}_{it}, E, \tau))^{-1/2}$.

2) Global Optimization: Given the optimal energy allocation weights $\boldsymbol{W}_{it}^*$ for all single sensors, we adopt global optimization to solve the optimal weight $\boldsymbol{W}^*$ for the entire system. Our goal is to find the vector with the highest similarity with the individual optimal solutions. We define the given $\boldsymbol{W}_{it}^*$s as vector set $\mathbb{V}$ and take the sum distances from $\boldsymbol{W}^*$ to $\mathbb{V}$ as the cost function. Then, $\boldsymbol{W}^*$ can be achieved by minimizing the cost. Considering that sensors contribute differently to the sum throughput, ρ_{it} is introduced as the contribution factor for $\hat{S}_{i,t}$. The global optimization problem is formed as:

$$\begin{aligned} (P5): \quad & \min_{\boldsymbol{W}} \sum_{i=1}^{N_V}\sum_{t=1}^{N_T} ||\rho_{it}(\boldsymbol{W} - \boldsymbol{W}_{it}^*)||_F^2 \\ & C1: \boldsymbol{W} \succeq \boldsymbol{W}^{lb}, \\ s.t. \quad & C2: \boldsymbol{W}\boldsymbol{W}^H = 1. \\ & C3: \boldsymbol{W} \preceq \boldsymbol{W}^{ub} \end{aligned} \tag{26}$$

We utilize the Frobenius norm to represent vector distances (or similarity) since it is effective in low-rank approximation [42], [43]. The Rayleigh quotient can be transformed into the quadratic form by scaling the denominator, and the throughput is a logarithmic function. We define

$$\lambda_{it} = \frac{\boldsymbol{W}_{it}^* \mathcal{Q}_{it}^n (\boldsymbol{W}_{it}^*)^H}{\boldsymbol{W}_{it}^* \mathcal{Q}_{it}^d (\boldsymbol{W}_{it}^*)^H}, \tag{27}$$

where $\mathcal{Q}_{it}^n$ and $\mathcal{Q}_{it}^d$ are normalized $\boldsymbol{Q}_{it}^n(\boldsymbol{B}_{it}, E, \tau)$ and $\boldsymbol{Q}_{it}^d(\boldsymbol{B}_{it}, E, \tau)$. A judicious contribution factor can be denoted as $\rho_{it} = \sqrt{log_2(\lambda_{it})}$.

Theorem 2: Defining $\rho = \sum_{i=1}^{N_V}\sum_{t=1}^{N_T}\rho_{it}^2$ and $R_k = \sum_{i=1}^{N_V}\sum_{t=1}^{N_T}(w_{it}^k)^*\rho_{it}^2$, then the solution of $(P5)$ can be written as

$$w_k^* = \begin{cases} w_k^{lb} & \varphi \geq \dfrac{R_k}{w_k^{lb}} - \rho, \\ \dfrac{R_k}{\rho + \varphi} & \dfrac{R_k}{w_k^{ub}} - \rho < \varphi < \dfrac{R_k}{w_k^{lb}} - \rho, \\ w_k^{ub} & \varphi \leq \dfrac{R_k}{w_k^{ub}} - \rho, \end{cases} \tag{28}$$

where the φ is parameter that enables $\boldsymbol{W}^*(\boldsymbol{W}^*)^H = 1$.

Proof. Please see Appendix B. □

C. Time segment factor optimization

To optimize τ, we define $\chi_{it} = \sum_{j=1}^{M_k}\sum_{k=1,k\neq i}^{N_V}\hat{\iota}_{kj,t}\hat{\kappa}_{kj,t}^i EN_T\eta\left|\boldsymbol{B}_{it}\boldsymbol{G}_{kj}^i\right|^2\left|\boldsymbol{W}\hat{\boldsymbol{H}}_{kj}\right|^2/\mu_{kj}$, $\psi_{it} = \sum_{j=1}^{M_i}\hat{\iota}_{ij,t}\hat{\kappa}_{ij,t}^i EN_T\eta\left|\boldsymbol{B}_{it}\boldsymbol{G}_{ij}^i\right|^2\left|\boldsymbol{W}\hat{\boldsymbol{H}}_{ij}\right|^2/\mu_{ij}$ and $\xi_{it} = T|\boldsymbol{B}_{it}|^2\sigma_{Ap}^2$, the optimization problem on τ can be written as

$$\begin{aligned} (P6): & \frac{\hat{\ell}_S T}{N_T}\max_{\tau} \sum_{i=1}^{N_V}\sum_{t=1}^{N_T}(1-\tau)log_2\left(1 + \frac{\psi_{it}}{\chi_{it} + (1-\tau)\xi_{it}}\right) \\ & C1: \quad \tau^{lb} \leq \tau < 1, \\ s.t. \quad & C2: \quad Max(\tfrac{w_i^2 E}{TP_{max}}) \leq \tau. \end{aligned} \tag{29}$$

$f(\tau) = (1-\tau)log_2\left(1 + \frac{\psi}{\chi + (1-\tau)\xi}\right)$ is monotonic decreasing over τ since its first derivative is negative when $\tau \in [0, 1]$. Thus the objective function, which is the non-negative sum of $f(\tau)$, is monotonic decreasing as well. Obviously, $\tau^* = Max(\tau^{lb}, \frac{w_i^2 E}{TP_{max}})$ if it is less than 1.

Algorithm 2 Joint alternating optimal solution

1: **Input:** $\boldsymbol{H}$, $\boldsymbol{G}$, P_{max}, η, and Υ_i
2: **Output:** $\boldsymbol{W}^*$, $\boldsymbol{B}^*$, E^* and τ^*;
3: **for** $itera = 1$ to 20, **do**
4: Obtain $\boldsymbol{W}_{it}^*$ according to Algorithm 1;
5: Obtain $\boldsymbol{W}^*$ according to (28), and update feasible region of τ and E according to (29), (30);
6: Set τ^* as $Max(\tau^{lb}, \frac{w_i^2 E}{TP_{max}})$
7: Set E as $Min(\frac{P_{max}\tau T}{w_i^2})$.
update $\boldsymbol{W}^{lb}$ according to (7);
8: Obtain $\boldsymbol{B}^*$ with (21);
9: Calculate throughput $\mathcal{T}_{itera}$;
10: **if** $(\mathcal{T}_{itera} - \mathcal{T}_{itera-1} \leq \delta)$
11: Return $\boldsymbol{W}^*$, $\boldsymbol{B}^*$, E^*, τ^* and terminate;
12: **end if**
13:**end for**

D. Rated energy consumption optimization

We define the constants $\theta_{it} = \sum_{j=1}^{M_k}\sum_{k=1,k\neq i}^{N_V} \hat{\iota}_{kj,t}\hat{\kappa}_{kj,t}^i N_T\eta \left|\boldsymbol{B}_{it}\boldsymbol{G}_{kj}^i\right|^2 \left|\boldsymbol{W}\hat{\boldsymbol{H}}_{kj}\right|^2/\mu_{kj}$, $\varpi_{it} = \sum_{j=1}^{M_i} \hat{\iota}_{ij,t}\hat{\kappa}_{ij,t}^i N_T\eta \left|\boldsymbol{B}_{it}\boldsymbol{G}_{ij}^i\right|^2 \left|\boldsymbol{W}\hat{\boldsymbol{H}}_{ij}\right|^2/\mu_{ij}$, and $\kappa_{it} = (1-\tau)T|\boldsymbol{B}_{it}|^2\sigma_{Ap}^2$, the optimization problem on E can be written as

$$(P7): \max_{E} \hat{\ell}_S\hat{\tau}\sum_{i=1}^{N_V}\sum_{t=1}^{N_T} log_2\left(1+\frac{\varpi_{it}E}{\theta_{it}E+\kappa_{it}}\right) \quad s.t. \quad \begin{array}{ll} C1: & E \geq Max(E_i^{lb}), \\ C2: & E \leq Min(\frac{P_{max}\tau T}{w_i^2}), \end{array} \tag{30}$$

where $C1$ is given in (8) and $C2$ draws from $P_{Ap}^i \leq P_{max}$. The function $f(E) = log_2\left(1+\frac{\varpi E}{\theta E+\kappa}\right)$ is monotonic increasing over E since its first derivative is positive when $E \in [0,\infty)$. Thus the objective function is monotonic increasing as well. It is obvious that the optimal E equals to $Min(\frac{P_{max}\tau T}{w_i^2})$ if it is greater than $Max(E_i^{lb})$.

E. Joint optimization

Based on the above inferences, we propose a joint alternating optimization algorithm as shown in Algorithm 2. It can be summarized as optimizing and updating variables alternately until convergence. δ is the convergence threshold. Although it is difficult to prove that the objective function is jointly concave strictly, an approximately optimal solution can be obtained. In practice, P_{max} and η are determined by the circuit, $\boldsymbol{H}$ and $\boldsymbol{G}$ can be estimated or modelled, and Υ_i depends on the traffic of AP_i. Based on the above information, a high-quality sub-optimal transmission strategy $\{E^*, \tau^*, \boldsymbol{P}_{Ap}^*, \boldsymbol{W}^*, \boldsymbol{B}^*\}$ is available for the wireless powered multi-network overlapping system.

The computational complexity of Algorithm 2 is dominated by the calculation of the $M \times N$ eigenvectors in $(P2)$ and $(P4)$, and the computational complexity is $\mathcal{O}(A^2)$ and $\mathcal{O}(N^2)$ respectively. Thus, the total complexity of Algorithm 2 can be approximately expressed as $\mathcal{O}(MN(A^2+N^2))$.

IV. Numerical Results

In this section, simulations are conducted to demonstrate our presented scheme in Section III. The performance of the proposed joint alternating optimization is discussed and compared with the separate optimizations. Then we make insight into the impact of diverse parameters and analyze the characteristics of the curves.

Without loss of generality, we assume that channel coefficients are modelled according to Rician fading in which the complex channel is given by

$$h = \left[\sqrt{\frac{m}{m+1}}h^{\text{LoS}} + \sqrt{\frac{1}{m+1}}h^{\text{NLoS}}\right]\sqrt{c_0\left(\frac{d}{d_0}\right)^{-v}},$$

where h^{LoS} is the line-of-sight (LoS) deterministic component with $|h^{LoS}|^2 = 1$, h^{NLoS} is a Gaussian random variable with zero mean and unit variance representing non-LoS Rayleigh fading component, m denotes the Rician factor, c_0 is a constant attenuation due to the path-loss at a reference distance d_0 , v is a path loss exponent and d is the distance between the transmitter and the receiver [45], [46]. Throughout the simulation, we consider $m = 3$, $c_0 = -20$dB, $d_0 = 1$, and $v = 3$.

We set $N = 10$, $M_i = 30$, $A = 5$ and $T = 1$ in the simulation. The convergence threshold δ is set as 0.01. To simulate the actual spatial locations, the distances from AP_i to S_{ij}, S_{kj} $(k \neq i)$ and MAP are randomly generated with uniform distribution $U(10,40)$, $U(30,60)$ and $U(900,1000)$. We assume that the traffic (Υ_i) between all HAPs and MAP is the same, thus can be denoted as Υ. The energy conversion ratio $\eta = 0.7$, and the power of noise σ_M^2, σ_{Ap}^2 and σ_S^2 is -110 dBm. As a contrast, $\boldsymbol{B}_R$ is an equal-weight receive vector, $\boldsymbol{W}_R$ and τ_R are randomly generated. Note that we identify the curves as $Curve\ A \sim Curve\ Z$ according to the legend from top to bottom for a simpler description.

A. The comparison between separate and joint optimization

Fig. 4 depicts the relationship between sum-throughput and the energy consumption E. In Fig. 4 (a), it is observed that $Curve\ D \sim Curve\ F$ keep rising as E increases until reaching the right boundary and is truncated then. The right boundary is caused by the maximum transmission power constraint $P_{Ap}^i \leq P_{max}$. At the jump point, $Max(P_{Ap}^i) = P_{max}$ holds, and it is inadvisable to keep increasing E. $Curve\ A \sim Curve\ C$ avoid the truncation with the optimization of τ, they show a trend of rising first and falling then. Thus there is a peak point at which the sum throughput of the system is maximized. The downward trend reflects the consequences of keeping increasing E forcibly after reaching the sub-optimal rated energy consumption (E^*). By comparing Fig. 4 (a) to Fig. 4 (c), it is apparent that with the increase of Υ, the peak value of $CurveA \sim CurveC$ keeps decreasing, and the corresponding energy consumption increases gradually, which is consistent with cognition. Particularly, when Υ rises from 2 to 5, the left boundary appears in Fig. 4 (b), which can be explained as the increase of Υ causes the constraint $r_i \geq \Upsilon_i$ unsatisfiable in the low energy area. As Υ increases, the

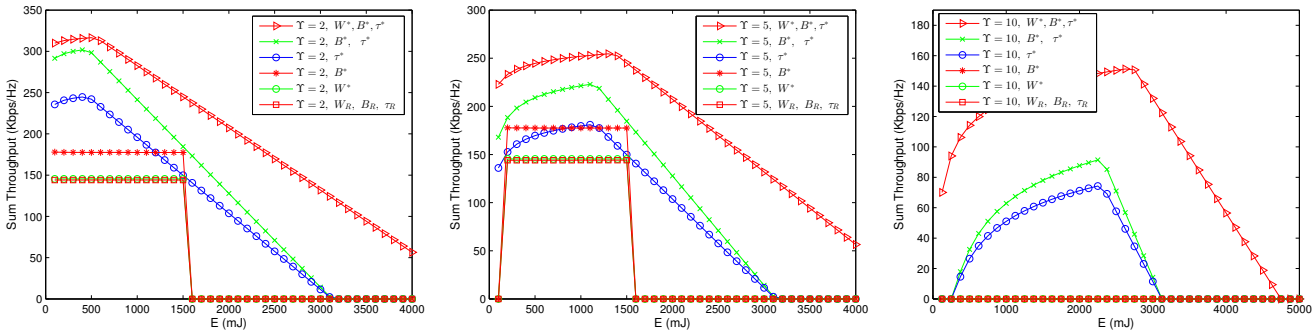

(a) $\Upsilon = 2$Kbit. (b) $\Upsilon = 5$Kbit. (c) $\Upsilon = 10$Kbit.

Fig. 4. Sum throughput in VANs versus the energy consumption E when $P_{max} = 2$ W, $\tau_R = 0.5$, Υ equals 2, 5, and 10 Kbit respectively.

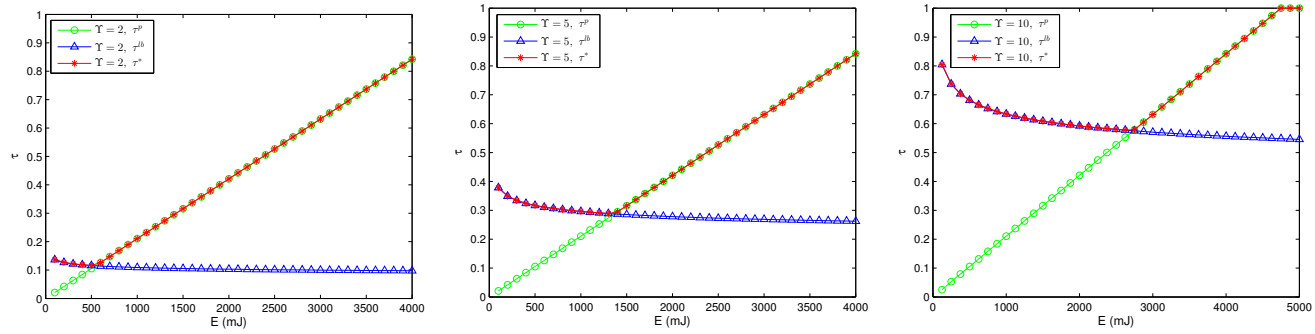

(a) $\Upsilon = 2$Kbit. (b) $\Upsilon = 5$Kbit. (c) $\Upsilon = 10$Kbit.

Fig. 5. Lower bounds and sub-optimal value of τ versus the energy consumption E when $P_{max} = 2$ W, $\tau_R = 0.5$, Υ equals 2, 5, and 10 Kbit respectively.

feasible range of E is further reduced. Furthermore, $Curve\ A$ in Fig. 4 (c) reflects that $\boldsymbol{W}$ enables the system to work with lower energy consumption in the joint optimization when Υ is high.

In brief, the proposed strategy always performs best in the entire interval. τ and $\boldsymbol{B}$ can effectively optimize the throughput. $\boldsymbol{W}$ performs poorly when optimized separately but is significant in joint optimization. τ and W can expand the feasible range of E. Besides, there is a suitable E^* that maximizes the throughput, and excessive energy will cause performance degradation.

B. The tendency of sub-optimal τ^*

In this section, we investigate how the boundary and sub-optimal value of τ changes with E. τ^{lb} and τ^p are two lower bounds of τ that guarantee $r_i \geq \Upsilon_i$ and $P_{Ap}^i \leq P_{max}$ respectively. Fig. 5 illustrates the tendency of τ^* as E increases when $\Upsilon = 2$, 5, and 10. The τ^* corresponding to the given E can be observed from the curves as well. It is noticed that τ^{lb} decreases, and τ^p increases gradually with E. On the left of the intersection, the lower bound of τ depends on τ^{lb}. τ is limited to guarantee the necessary throughput from HAPs to MAP. As E increases, τ^* reaches the valley value at the intersection. In this case, at least one HAP transmits signals at P_{max} and the valley points here correspond to the peak points in Fig. 4. On the right of the intersection, τ^p determines the lower bound of τ. The HAPs keep transmitting signals with

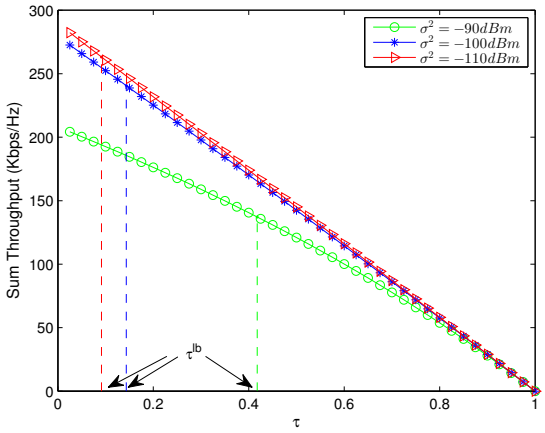

Fig. 6. Sum throughput versus τ when $P_{max} = 0.5$ W, $E = 5$ mJ, $\Upsilon = 1$ Kbit, σ^2 equals to -110, -100, and -90 dBm respectively.

P_{max} and τ goes up to consume all energy. When Υ rises, $Curve\ B$ moves up, and the intersection moves to the right.

In short, the τ^* depends on its two lower bounds. It decreases first and then increases with E. The coordinates of the intersection point are τ^* and E^*, which corresponds to the peak throughput.

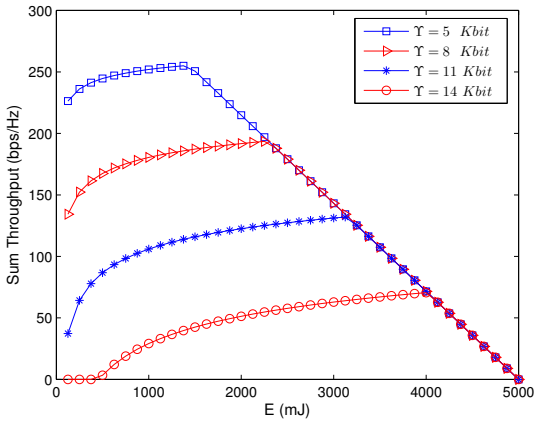

(a) Sum throughput versus E.

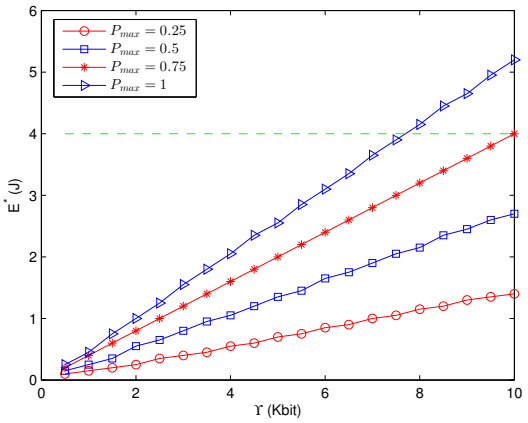

(b) E^* versus Υ_i

Fig. 7. Impact of constraint Υ on energy consumption E and sum throughput under joint optimization.

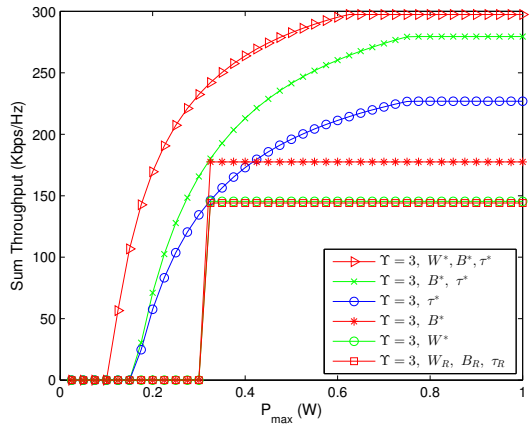

(a) Available peak throughput versus P_{max}.

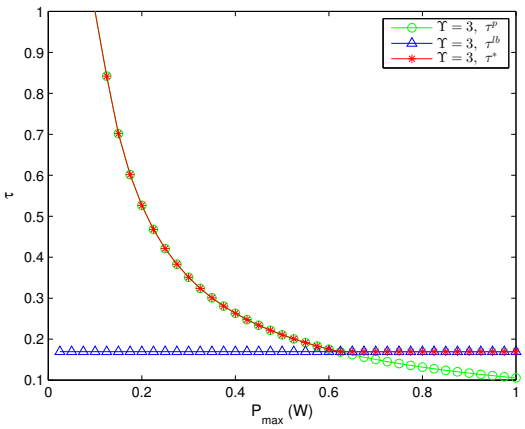

(b) The lower bounds and sub-optimal τ versus P_{max}.

Fig. 8. Available peak throughput and sub-optimal τ versus the maximum transmission power P_{max} when $E = 1$J, $\Upsilon = 3$ Kbit.

C. The impact of time segment factor τ

In Fig. 6, the available sum throughput versus the time segment factor τ is studied. We set $E = 5$ mJ, $P_{max} = 2$W and $\Upsilon = 1$ Kbit in the simulation. Consistent with the theoretical derivation, the objective function is monotonic decreasing in the range $[0, 1]$ and reaches 0 when $\tau = 1$. When we set the single antenna noise power $\sigma^2 = \sigma_S^2 = \sigma_{Ap}^2 = \sigma_M^2$ as -90, -100, and -110 dBm, τ gets the sub-optimal value $\tau^* = 0.42$, 0.14 and 0.09 respectively, which are the lower bound of τ as well. Note that the curve on the left of τ^* is only plotted to verify the monotonicity, the values less than τ^* are inaccessible in practice.

The results suggest that optimizing τ is significant in improving the performance since the sum throughput decreases almost linearly with τ, which also leads to the fact that some curves appear to be approximately linear in our simulation results.

D. The impact of throughput constraint Υ

Fig. 7. (a) illustrates the main characteristics of the throughput performance as the function of E under different Υ. When Υ increases from 5 to 14, there is an apparent decrease in sum throughput and more energy is required to reach the peak throughput. The relationship between the sub-optimal energy and Υ is shown more intuitively in Fig. 7. (b), where the influence of maximum transmission power P_{max} is also considered. In practice, the maximum available energy should also be considered. If there is an energy upper bound as shown by the green dotted line in Fig. 7. (b), the P_{max} and E should be set reasonably rather than increasing indefinitely.

In general, the more energy is required to obtain the peak throughput. The sum throughput and energy increase or decrease approximately linearly. Increasing E and P_{max} simultaneously is an effective method to improve the sum throughput under high Υ constraints.

E. The impact of maximum transmission power P_{max}

Fig. 8 illustrates the trend of sum throughput and time segment factor with P_{max}. We set $\Upsilon = 3$ Kbit and $E = 1$J. It is observed that τ^p is inversely proportional to P_{max}, and τ^{lb} is a constant independent of P_{max}. When $P_{max} < 0.125$, even if HAPs transmit signals with P_{max}, the given energy cannot

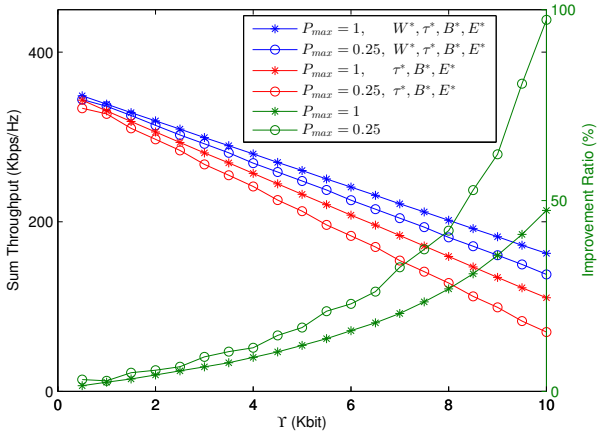

Fig. 9. The sum throughput and improvement ratio versus Υ, joint optimizations with and without $\boldsymbol{W}$ are compared.

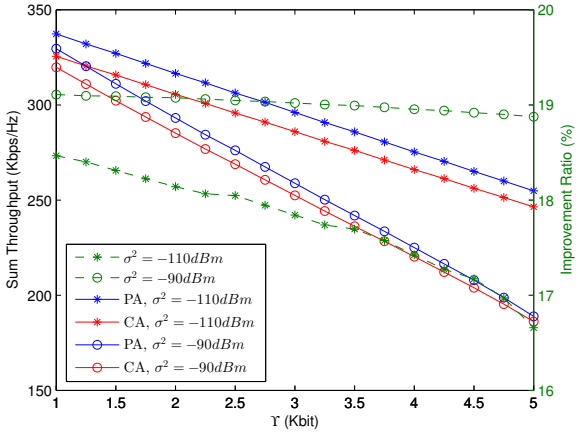

Fig. 10. The sum throughput and improvement ratio versus Υ, FA and CA are compared.

be completely consumed in single time block, so τ^p exceeds the upper bound $\tau = 1$. Thanks to the joint optimization, $Curve\ A$ starts to rise earlier than others and always performs best. The sum throughput increases with P_{max} until P_{max} reaches 0.625. It should be noted that $CurvesB$ and C show the same trend, but due to their lack of optimization on W, higher P_{max} values are required to reach their performance upper bounds. After that, the lower bound of τ is determined by τ^{lb}, which is unrelated to P_{max}, so increasing P_{max} does not work anymore. Moreover, $Curve\ B$ and $Curve\ C$ begin to rise from zero at $P = 0.15$ with the optimization of τ, and a higher P_{max} is required for $Curve\ D \sim Curve\ F$. The minimum acceptable P_{max} for the system is $Max(w_i^2 E/T)$.

It can be inferred that P_{max} has to exceed a certain threshold that enables the system to work. The sum throughput increases continuously with P_{max}, and increasing P_{max} is no longer effective after $\tau^{lb} > \tau^p$.

F. The impact of energy allocation weight $\boldsymbol{W}$ in joint optimization

As reflected in $Section\ A$ and $Section\ E$, $\boldsymbol{W}$ is well-performed in expanding the feasible interval of E and P_{max}. In Fig. 9, the joint optimizations with and without $\boldsymbol{W}$ are compared to investigate their effect on improving the sum throughput. The improvement ratio in $Curve\ E$ is defined as $(Curve\ A - Curve\ C)/Curve\ C$. We notice that the sum throughput declines slower with the optimization of $\boldsymbol{W}$, and its improvement ratio is more remarkable with the increase of Υ. Besides, when $\Upsilon = 10$ and P_{max} decreases from 1 to 0.25, the improvement ratio increases from 47% to 97%. Both increasing P_{max} and optimizing W can slow down the decreasing trend of optimal throughput, and the effect obtained by optimizing W is more prominent under the preset parameters.

The above phenomena indicate that $\boldsymbol{W}$ has a more noticeable effect under severe conditions (e.g., lower E, P_{max}, and higher Υ).

G. Comparison with related works

To further verify the effectiveness of the proposed algorithm (PA), we compare it with the algorithm (CA) [47] under different noise parameters. The improvement ratio in $Curve\ A$ is defined as $(Curve\ C - Curve\ D)/Curve\ D$. It can be seen from Fig. 10 that under different constraints Υ, PA always has better performance than CA. The reason for the decrease in performance improvement ratio is that the increase of Υ shrinks the value range of optimization variables, and the optimal solutions of PA and CA tend to be similar, resulting in a gradual weakening of the effect of optimization. In addition, by observing the performance improvement ratio, it can be found that when the noise power is higher, the improvement ratio of PA is more gradual, which further verifies the performance stability of the proposed algorithm under harsh conditions.

In brief, Fig. 10 illustrates the effectiveness of the proposed algorithm from double perspectives by changing the independent variables Υ and σ^2.

V. Conclusion

This paper investigates the transmission strategy for a wireless powered multi-VAN system, which enables vehicles to transfer the power to the sensors while communicating with the remote MAP. Sensors recycle the RF energy from HAPs and then transmit sensing data to the intended HAP via FTDMA. Both the extra energy and interference induced by multiple VANs are considered. We jointly optimize the energy consumption (E), time segment factor (τ), transmission power ($\boldsymbol{P}_{Ap}$), energy allocation weights ($\boldsymbol{W}$), and receive beamforming ($\boldsymbol{B}$) to maximize the sum-throughput of all the sensors. High-quality sub-optimal strategy $\pi^* = \{E^*, \tau^*, \boldsymbol{P}_{Ap}^*, \boldsymbol{W}^*, \boldsymbol{B}^*\}$ is obtained by the alternating optimization method. Simulation results illustrate the advantages of the proposed scheme.

Appendix A
Proof of the Proposition 1

First, we abbreviate $\boldsymbol{Q}_{it}^d(\boldsymbol{B}_{it}, E, \tau)$ and $\boldsymbol{Q}_{it}^n(\boldsymbol{B}_{it}, E, \tau)$ as $\boldsymbol{Q}_{it}^d$ and $\boldsymbol{Q}_{it}^n$. For generalization, we omit all subscripts (i.e.,

it) later, and the number of HAPs (N_V) is shortened as N. The objective function of $(P4)$ is a generalized Rayleigh quotient. Defining that $\boldsymbol{K}=[k_1,k_2,\cdots,k_N]=\boldsymbol{W}(\boldsymbol{Q}^d)^{1/2}$ and $\boldsymbol{Q}=(\boldsymbol{Q}^d)^{-1}\boldsymbol{Q}^n$, then $(P4)$ can be written in standard form

$$\begin{aligned}(P8):\quad \max_{\boldsymbol{K}}\ & \frac{\boldsymbol{K}\boldsymbol{Q}\boldsymbol{K}^H}{\boldsymbol{K}\boldsymbol{K}^H}\\ & C1:\boldsymbol{K}\succeq\boldsymbol{W}^{lb}\ (\boldsymbol{Q}^d)^{1/2},\\ s.t.\quad & C2:\boldsymbol{K}\boldsymbol{K}^H=\zeta,\\ & C3:\boldsymbol{K}^{ub}\preceq\boldsymbol{W}^{ub}\ (\boldsymbol{Q}^d)^{1/2}.\end{aligned}\tag{31}$$

The Lagrangian function of $(P8)$ and its KKT conditions are given by

$$\begin{aligned}L(\boldsymbol{K},\boldsymbol{\alpha},\boldsymbol{\varrho},\beta)=&\frac{1}{\zeta}\boldsymbol{K}\boldsymbol{Q}\boldsymbol{K}^H-\boldsymbol{\alpha}\Big[\boldsymbol{K}-\boldsymbol{W}^{lb}(\boldsymbol{Q}^d)^{1/2}\Big]^H\\&+\boldsymbol{\varrho}\Big[\boldsymbol{K}-\boldsymbol{W}^{ub}(\boldsymbol{Q}^d)^{1/2}\Big]^H-\beta\left[\boldsymbol{K}\boldsymbol{K}_{ij}^H-\zeta\right],\end{aligned}\tag{32}$$

$$\boldsymbol{Q}\boldsymbol{K}^*-\hat{\beta}\boldsymbol{K}^*-\hat{\boldsymbol{\alpha}}+\hat{\boldsymbol{\varrho}}=\boldsymbol{0}_{1\times N},\tag{33}$$

$$\boldsymbol{K}^*-\boldsymbol{W}^{lb}(\boldsymbol{Q}^d)^{1/2}\succeq\boldsymbol{0}_{1\times N},\tag{34}$$

$$\boldsymbol{K}^*-\boldsymbol{W}^{ub}(\boldsymbol{Q}^d)^{1/2}\preceq\boldsymbol{0}_{1\times N},\tag{35}$$

$$\boldsymbol{K}^*(\boldsymbol{K}^*)^H=\zeta,\tag{36}$$

$$\boldsymbol{\alpha}\succeq\boldsymbol{0}_{1\times N},\boldsymbol{\varrho}\succeq\boldsymbol{0}_{1\times N},\tag{37}$$

$$\boldsymbol{\alpha}\Big[\boldsymbol{K}^*-\boldsymbol{W}^{lb}(\boldsymbol{Q}^d)^{1/2}\Big]^H=0,\tag{38}$$

$$\boldsymbol{\varrho}\Big[\boldsymbol{K}^*-\boldsymbol{W}^{ub}(\boldsymbol{Q}^d)^{1/2}\Big]^H=0,\tag{39}$$

where $\boldsymbol{\alpha},\boldsymbol{\varrho},\beta$ are Lagrangian coefficients, and $\hat{\boldsymbol{\alpha}}=\boldsymbol{\alpha}\zeta/2$ $\hat{\boldsymbol{\varrho}}=\boldsymbol{\varrho}\zeta/2$, $\hat{\beta}=\beta\zeta$.

According to (33)-(39), the conditions for sub-optimal solution $\boldsymbol{K}^*$ can be simplified as: $\boldsymbol{K}^*-\boldsymbol{W}^{lb}(\boldsymbol{Q}^d)^{1/2}\succeq\boldsymbol{0}_{1\times N}$, $\boldsymbol{W}^{ub}(\boldsymbol{Q}^d)^{1/2}-\boldsymbol{K}^*\succeq\boldsymbol{0}_{1\times N}$ and $\boldsymbol{Q}\boldsymbol{K}^*-\hat{\beta}\boldsymbol{K}^*=\boldsymbol{0}_{1\times N}$. We solve $\boldsymbol{Q}\boldsymbol{K}^*=\hat{\beta}\boldsymbol{K}^*$ first and get the solution $\tilde{\boldsymbol{K}}=Eigmaxv(\boldsymbol{Q})$. To avoid calculating ζ, we transfer $\tilde{\boldsymbol{K}}$ to $\tilde{\boldsymbol{W}}$ temporarily. $\tilde{\boldsymbol{W}}=[\tilde{w}_1,\tilde{w}_2,\cdots,\tilde{w}_N]$ is defined as

$$\tilde{\boldsymbol{W}}=\frac{\tilde{\boldsymbol{K}}(\boldsymbol{Q}^d)^{-1/2}}{|\tilde{\boldsymbol{K}}(\boldsymbol{Q}^d)^{-1/2}|^2}.\tag{40}$$

$\boldsymbol{K}^{lb}=[k_1^{lb},k_2^{lb},\cdots,k_N^{lb}]=\boldsymbol{W}^{lb}(\boldsymbol{Q}^d)^{1/2}$ and $\boldsymbol{K}^{ub}=[k_1^{ub},k_2^{ub},\cdots,k_N^{ub}]=\boldsymbol{W}^{ub}(\boldsymbol{Q}^d)^{1/2}$ are the lower and upper bounds of $\boldsymbol{K}$ according to (26). Then we consider the following cases: First, if $\boldsymbol{W}^{lb}\preceq\tilde{\boldsymbol{W}}\preceq\boldsymbol{W}^{ub}$, there is $\boldsymbol{K}^*=\tilde{\boldsymbol{K}}$. Second, if $\tilde{\boldsymbol{W}}\preceq\boldsymbol{W}^{lb}$ or $\tilde{\boldsymbol{W}}\succeq\boldsymbol{W}^{ub}$, $\boldsymbol{K}^*$ is unsolvable since (34) or (35) cannot be satisfied at all events. Otherwise, we fix element ${k_i}^*$ as k_i^{lb} if $\tilde{w}_i<w_i^{lb}$ or k_i^{ub} if $\tilde{w}_i>w_i^{ub}$ (same as done in the water-filling algorithm [44]). Then, other elements of $\boldsymbol{K}^*$ can be calculated with the modified matrix $\mathcal{A}$ via $Eigmaxv(\mathcal{A})$. The conversion process from $\boldsymbol{Q}$ to $\mathcal{A}$ is as follows:

First, we express $\boldsymbol{Q}\boldsymbol{K}=\hat{\beta}\boldsymbol{K}$ in matrix form

$$\begin{bmatrix}q_{11}&q_{12}&\cdots&q_{1N}\\q_{21}&q_{22}&\cdots&q_{2N3}\\\vdots&\vdots&\ddots&\vdots\\q_{N1}&q_{N2}&\cdots&q_{NN}\end{bmatrix}\begin{bmatrix}k_1\\k_2\\\cdots\\k_N\end{bmatrix}=\hat{\beta}\begin{bmatrix}k_1\\k_2\\\cdots\\k_N\end{bmatrix}.\tag{41}$$

Considering the case that only the first element needs to be fixed as k_1^{lb}, we give the equivalent expression as

$$\begin{bmatrix}q_{11}&q_{12}\frac{k_1^{lb}}{k_1}&\cdots&q_{1N}\frac{k_1^{lb}}{k_1}\\q_{21}\frac{k_1}{k_1^{lb}}&q_{22}&\cdots&q_{2N}\\\vdots&\vdots&\ddots&\vdots\\q_{N1}\frac{k_1}{k_1^{lb}}&q_{N2}&\cdots&q_{NN}\end{bmatrix}\begin{bmatrix}k_1^{lb}\\k_2\\\cdots\\k_N\end{bmatrix}=\hat{\beta}\begin{bmatrix}k_1^{lb}\\k_2\\\cdots\\k_N\end{bmatrix}.\tag{42}$$

We express (42) as $\hat{\boldsymbol{K}}\mathcal{A}=\hat{\beta}\hat{\boldsymbol{K}}$ and define $\mathcal{A}=\boldsymbol{Q}\odot\mathcal{P}_1$. Here the operator $\odot$ represents the Hadamard product. $\mathcal{P}_i$ is an all-one matrix if $\boldsymbol{W}^{lb}\preceq\tilde{\boldsymbol{W}}\preceq\boldsymbol{W}^{ub}$. Otherwise, multiply the ith row by k_i/k_i^{ub} (or k_i/k_i^{lb}) and the ith column by k_i^{ub}/k_i (or k_i^{lb}/k_i) if $\tilde{w}_i<w_i^{lb}$ ($\tilde{w}_i>w_i^{ub}$). Here is an example for case $\tilde{w}_1<w_1^{lb}$.

$$\mathcal{P}_1=\begin{bmatrix}1&\frac{k_1}{k_1^{lb}}&\cdots&\frac{k_1}{k_1^{lb}}\\\frac{k_1^{lb}}{k_1}&1&\cdots&1\\\vdots&\vdots&\ddots&\vdots\\\frac{k_1^{lb}}{k_1}&1&\cdots&1\end{bmatrix}.\tag{43}$$

Denote the element at column i, row m of $\mathcal{A}$ as $\mathcal{A}^{mi}$. k_i^* can be present as $(\sum_{m=1,m\neq i}^{N}\mathcal{A}^{mi}k_m^*)/(\hat{\beta}-\mathcal{A}^{kk})$ if $w_i^{lb}\leq\tilde{w}_i\leq w_i^{ub}$, w_i^{lb} if $\tilde{w}_i<w_i^{lb}$ and w_i^{ub} if $\tilde{w}_i>w_i^{ub}$ according to (42).

Appendix B
Proof of the Proposition 2

The Lagrangian function of $(P5)$ and its KKT conditions are given by

$$\begin{aligned}L(\boldsymbol{W},\boldsymbol{\nu},\varphi)=&\sum_{i=1}^{N}\sum_{j=1}^{M}\|\rho_{it}(\boldsymbol{W}-\boldsymbol{W}_{it}^*)\|_F^2+\boldsymbol{\nu}\left(\boldsymbol{W}^{ub}-\boldsymbol{W}\right)^H\\&+\boldsymbol{\gamma}\left(\boldsymbol{W}-\boldsymbol{W}^{lb}\right)^H+\varphi\left(\boldsymbol{W}^H\boldsymbol{W}-1\right),\end{aligned}\tag{44}$$

$$\sum_{i=1}^{N}\sum_{j=1}^{M}2\rho_{it}^2(\boldsymbol{W}^*-\boldsymbol{W}_{it}^*)-\boldsymbol{\nu}+\boldsymbol{\gamma}+2\varphi\boldsymbol{W}^*=\boldsymbol{0}_{1\times N},\tag{45}$$

$$\boldsymbol{W}^{lb}-\boldsymbol{W}^*\preceq\boldsymbol{0}_{1\times N},\tag{46}$$

$$\boldsymbol{W}^{ub}-\boldsymbol{W}^*\succeq\boldsymbol{0}_{1\times N},\tag{47}$$

$$\boldsymbol{\nu}^*\succeq\boldsymbol{0}_{1\times N},\boldsymbol{\gamma}^*\succeq\boldsymbol{0}_{1\times N},\tag{48}$$

$$\boldsymbol{W}^*(\boldsymbol{W}^*)^H=1,\tag{49}$$

$$\boldsymbol{\nu}^*\left(\boldsymbol{W}^{lb}-\boldsymbol{W}^*\right)^H=0,\tag{50}$$

$$\boldsymbol{\gamma}^*\left(\boldsymbol{W}^{ub}-\boldsymbol{W}^*\right)^H=0,\tag{51}$$

where $\boldsymbol{\nu},\varphi$ are Lagrangian coefficients. Considering (45)-(51), the conditions for $\boldsymbol{W}^*$ can be described as: $\sum_{i=1}^{N}\sum_{j=1}^{M}2\rho_{it}^2(\boldsymbol{W}^*-\boldsymbol{W}_{it}^*)+2\varphi\boldsymbol{W}^*=\boldsymbol{0}_{1\times N}$, $\boldsymbol{W}^*-\boldsymbol{W}^{lb}\succeq\boldsymbol{0}_{1\times N}$ and $\boldsymbol{W}^{ub}-\boldsymbol{K}^*\succeq\boldsymbol{0}_{1\times N}$. Defining $R_k=\sum_{i=1}^{N}\sum_{j=1}^{M}(w_{it}^k)^*\rho_{it}^2$ and $\rho=\sum_{i=1}^{N}\sum_{j=1}^{M}\rho_{it}^2$, the solution can be expressed as

$$w_k^*=\begin{cases}w_k^{lb} & \varphi\geq\dfrac{R_k}{w_k^{lb}}-\rho,\\ \dfrac{R_k}{\rho+\varphi} & \dfrac{R_k}{w_k^{ub}}-\rho<\varphi<\dfrac{R_k}{w_k^{lb}}-\rho,\\ w_k^{ub} & \varphi\leq\dfrac{R_k}{w_k^{ub}}-\rho,\end{cases}\tag{52}$$

REFERENCES

[1] Q. Qi, X. Chen, C. Zhong, and Z. Zhang, "Integration of energy, computation and communication in 6g cellular internet of things," *IEEE Communications Letters*, vol. 24, no. 6, pp. 1333–1337, 2020.

[2] B. Mao, Y. Kawamoto, and N. Kato, "AI-based joint optimization of QoS and security for 6G energy harvesting internet of things," *IEEE Internet of Things Journal*, vol. 7, no. 8, pp. 7032–7042, 2020.

[3] J. Liu, K. Xiong, P. Fan, and Z. Zhong, "RF energy harvesting wireless powered sensor networks for smart cities," *IEEE Access*, vol. 5, pp. 9348–9358, 2017.

[4] X. Zhang, K. Liu, and L. Tao, "A cooperative communication scheme for full-duplex simultaneous wireless information and power transfer wireless body area networks," *IEEE Sensors Letters*, vol. 2, no. 4, pp. 1–4, 2018.

[5] P. Wu, F. Xiao, H. Huang, C. Sha, and S. Yu, "Adaptive and extensible energy supply mechanism for uavs-aided wireless-powered internet of things," *IEEE Internet of Things Journal*, vol. 7, no. 9, pp. 9201–9213, 2020.

[6] M. Min, X. Wan, L. Xiao, Y. Chen, M. Xia, D. Wu, and H. Dai, "Learning-based privacy-Aware offloading for healthcare IoT with energy harvesting," *IEEE Internet of Things Journal*, vol. 6, no. 3, pp. 4307–4316, 2019.

[7] L. Xie, Y. Shi, Y. T. Hou, and A. Lou, "Wireless power transfer and applications to sensor networks," *IEEE Wireless Communications*, vol. 20, no. 4, pp. 140–145, 2013.

[8] X. Lu, P. Wang, D. Niyato, D. I. Kim, and Z. Han, "Wireless networks with RF energy harvesting: A contemporary survey," *IEEE Communications Surveys Tutorials*, vol. 17, no. 2, pp. 757–789, 2015.

[9] S. Verma, Y. Kawamoto, and N. Kato, "Energy-efficient group paging mechanism for QoS constrained mobile IoT devices over LTE-A pro networks under 5G," *IEEE Internet of Things Journal*, vol. 6, no. 5, pp. 9187–9199, 2019.

[10] A. Ghazanfari, H. Tabassum, and E. Hossain, "Ambient rf energy harvesting in ultra-dense small cell networks: performance and tradeoffs," *IEEE Wireless Communications*, vol. 23, no. 2, pp. 38–45, 2016.

[11] A. Rauniyar, P. E. Engelstad, and O. N. Østerbø, "On the performance of bidirectional noma-swipt enabled iot relay networks," *IEEE Sensors Journal*, vol. 21, no. 2, pp. 2299–2315, 2021.

[12] J. Tang, D. K. C. So, N. Zhao, A. Shojaeifard, and K.-K. Wong, "Energy efficiency optimization with swipt in MIMO broadcast channels for internet of things," *IEEE Internet of Things Journal*, vol. 5, no. 4, pp. 2605–2619, 2018.

[13] L. Liu, R. Zhang, and K.-C. Chua, "Wireless information and power transfer: A dynamic power splitting approach," *IEEE Transactions on Communications*, vol. 61, no. 9, pp. 3990–4001, 2013.

[14] Z. Ling, F. Hu, and M. Shao, "The optimal control policy for point-to-point wireless body area network based on simultaneous time-ratio and transmission power allocation," *IEEE Access*, vol. 7, pp. 46 454–46 460, 2019.

[15] H. Liu, F. Hu, S. Qu, Z. Li, and D. Li, "Multi-point wireless information and power transfer to maximize sum-throughput in WBAN with energy harvesting," *IEEE Internet of Things Journal*, vol. 6, no. 4, pp. 7069–7078, 2019.

[16] Z. Ling, F. Hu, Y. Zhang, L. Fan, F. Gao, and Z. Han, "Distributionally robust chance-constrained backscatter communication-assisted computation offloading in wbans," *IEEE Transactions on Communications*, vol. 69, no. 5, pp. 3395–3408, 2021.

[17] R. Zhang and C. K. Ho, "MIMO broadcasting for simultaneous wireless information and power transfer," *IEEE Transactions on Wireless Communications*, vol. 12, no. 5, pp. 1989–2001, 2013.

[18] X. Zhou, R. Zhang and C. K. Ho, "Wireless information and power transfer: Architecture design and rate-energy tradeoff," *IEEE Transactions on Communications*, vol. 61, no. 11, pp. 4754-4767, 2013.

[19] H. Ju and R. Zhang, "Throughput maximization in wireless powered communication networks," *IEEE Transactions on Wireless Communications*, vol. 13, no. 1, pp. 418–428, 2014.

[20] J. Tang, J. Song, J. Ou, J. Luo, X. Zhang, and K.-K. Wong, "Minimum throughput maximization for multi-uav enabled wpcn: A deep reinforcement learning method," *IEEE Access*, vol. 8, pp. 9124–9132, 2020.

[21] D. Song, W. Shin, J. Lee, and H. V. Poor, "Sum-throughput maximization in noma-based wpcn: A cluster-specific beamforming approach," *IEEE Internet of Things Journal*, vol. 8, no. 13, pp. 10 543–10 556, 2021.

[22] Y. Chen, N. Zhao, and M. Alouini, "Wireless energy harvesting using signals from multiple fading channels," *IEEE Transactions on Communications*, vol. 65, no. 11, pp. 5027–5039, 2017.

[23] Q. Sun, G. Zhu, C. Shen, X. Li, and Z. Zhong, "Joint beamforming design and time allocation for wireless powered communication networks," *IEEE Communications Letters*, vol. 18, no. 10, pp. 1783–1786, 2014.

[24] L. Liu, R. Zhang, and K. Chua, "Multi-antenna wireless powered communication with energy beamforming," *IEEE Transactions on Communications*, vol. 62, no. 12, pp. 4349–4361, 2014.

[25] B. Mao, Y. Kawamoto, J. Liu, and N. Kato, "Harvesting and threat aware security configuration strategy for ieee 802.15.4 based iot networks," *IEEE Communications Letters*, vol. 23, no. 11, pp. 2130–2134, 2019.

[26] Q. Qi, X. Chen, and D. W. K. Ng, "Robust beamforming for NOMA-based cellular massive IoT with SWIPT," *IEEE Transactions on Signal Processing*, vol. 68, pp. 211–224, 2020.

[27] M. Wu, Q. Song, L. Guo, and A. Jamalipour, "Joint user pairing and resource allocation in a swipt-enabled cooperative noma system," *IEEE Transactions on Vehicular Technology*, vol. 70, no. 7, pp. 6826–6840, 2021.

[28] S. Gong, S. Ma, C. Xing, and G. Yang, "Optimal beamforming and time allocation for partially wireless powered sensor networks with downlink SWIPT," *IEEE Transactions on Signal Processing*, vol. 67, no. 12, pp. 3197–3212, 2019.

[29] Q. Qi and X. Chen, "Wireless powered massive access for cellular internet of things with imperfect SIC and non-linear EH," *IEEE Internet of Things Journal*, vol. 6, no. 2, pp. 3110–3120, 2019.

[30] B. Mao, F. Tang, Y. Kawamoto, and N. Kato, "AI models for green communications towards 6G," *IEEE Communications Surveys Tutorials*, pp. 1–1, 2021.

[31] Z. Mao, F. Hu, D. Sun, S. Ma, and X. Liu, "Fairness-aware intragroup cooperative transmission in wireless powered communication networks," *IEEE Transactions on Vehicular Technology*, vol. 69, no. 6, pp. 6463–6472, 2020.

[32] Z. Chen, L. Qiu, and X. Liang, "Energy-efficient combination of small cells and multi-antenna under separation architecture," *IEEE Communications Letters*, vol. 19, no. 9, pp. 1572–1575, 2015.

[33] H. Zhang, H. Liu, J. Cheng, and V. C. M. Leung, "Downlink energy efficiency of power allocation and wireless backhaul bandwidth allocation in heterogeneous small cell networks," *IEEE Transactions on Communications*, vol. 66, no. 4, pp. 1705–1716, 2018.

[34] M. Ismail, K. Qaraqe, and E. Serpedin, "Cooperation incentives and downlink radio resource allocation for green communications in a heterogeneous wireless environment," *IEEE Transactions on Vehicular Technology*, vol. 65, no. 3, pp. 1627–1638, 2016.

[35] S. Guo, F. Wang, Y. Yang, and B. Xiao, "Energy-efficient cooperative tfor simultaneous wireless information and power transfer in clustered wireless sensor networks," *IEEE Transactions on Communications*, vol. 63, no. 11, pp. 4405–4417, 2015.

[36] H. Kim, H. Lee, L. Duan, and I. Lee, "Sum-rate maximization methods for wirelessly powered communication networks in interference channels," *IEEE Transactions on Wireless Communications*, vol. 17, no. 10, pp. 6464–6474, 2018.

[37] O. Rezaei, M. M. Naghsh, Z. Rezaei, and R. Zhang, "Throughput optimization for wireless powered interference channels," *IEEE Transactions on Wireless Communications*, vol. 18, no. 5, pp. 2464–2476, 2019.

[38] X. Zhou, J. Guo, S. Durrani and I. Krikidis, "Performance of Maximum Ratio Transmission in Ad Hoc Networks With SWIPT," *IEEE Wireless Communications Letters*, vol. 4, no. 5, pp. 529-532, 2015.

[39] T. K. Y. Lo, "Maximum ratio transmission," *IEEE Transactions on Communications*, vol. 47, no. 10, pp. 1458-1461, 1999.

[40] E. Boshkovska, D. W. K. Ng, N. Zlatanov, A. Koelpin, and R. Schober, "Robust resource allocation for MIMO wireless powered communication networks based on a non-linear eh model," *IEEE Transactions on Communications*, vol. 65, no. 5, pp. 1984–1999, 2017.

[41] M. He, F. Hu, Z. Ling, Z. Mao, and Z. Huang, "A dynamic weights algorithm on information and energy transmission protocol based on wban," *IEEE Transactions on Vehicular Technology*, vol. 70, no. 2, pp. 1528–1537, 2021.

[42] Y. Huang, G. Liao, Y. Xiang, L. Zhang, J. Li, and A. Nehorai, "Low-rank approximation via generalized reweighted iterative nuclear and frobenius norms," *IEEE Transactions on Image Processing*, vol. 29, pp. 2244–2257, 2020.

[43] X. Peng, C. Lu, Z. Yi, and H. Tang, "Connections between nuclear-norm and frobenius-norm-based representations," *IEEE Transactions on Neural Networks and Learning Systems*, vol. 29, no. 1, pp. 218–224, 2018.

[44] A. Liu, Y. Liu, H. Xiang, and W. Luo, "Polite water-filling for weighted sum-rate maximization in MIMO b-mac networks under multiple linear constraints," *IEEE Transactions on Signal Processing*, vol. 60, no. 2, pp. 834–847, 2012.

[45] L. Bai, Z. Huang, Y. Li and X. Cheng, "A 3D Cluster-Based Channel Model for 5G and Beyond Vehicle-to-Vehicle Massive MIMO Channels," *IEEE Transactions on Vehicular Technology*, vol. 70, no. 9, pp. 8401-8414, 2021.
[46] O. Rezaei, M. M. Naghsh, Z. Rezaei and R. Zhang, "Throughput Optimization for Wireless Powered Interference Channels," *IEEE Transactions on Wireless Communications*, vol. 18, no. 5, pp. 2464-2476, 2019.
[47] D. Hwang, D. I. Kim and T. J. Lee, "Throughput Maximization for Multiuser MIMO Wireless Powered Communication Networks," *IEEE Transactions on Vehicular Technology*, vol. 65, no. 7, pp. 5743-5748, 2016.

Chi Jin received the B.S. degree from the College of Communication Engineering, Jilin University, Changchun, Jilin, China, in 2019. He is currently pursuing the M.S. degree with the Information and Signal Processing Laboratory, College of Communication Engineering, Jilin University. His research interests include wireless body area networks and wireless power and information transfer.

Fengye Hu received the B.S. degree from the Department of Precision Instrument, Xian University of Technology (China) in 1996, and the M.S. and Ph.D. degrees in communication and information systems from Jilin University, China, in 2000 and 2007, respectively. He served as a visiting scholar in electrical and electronic engineering from Nanyang Technological University (NTU), Singapore, in 2011. He is currently a full professor in the College of Communication Engineering, Jilin University.

His current research interests include wireless body area networks, wireless energy and information transfer, energy harvesting, cognitive radio and space–time communication. He is an Editor of IET Communications and China Communications, and is an Editor of Physical Communication on Special Issue on Ultra-Reliable, Low-Latency and Low-Power Transmissions in the Era of Internet-of-Things. He has published 50 publications in IEEE journals and conferences. He organized the first and second Asia-Pacific Workshop on Wireless Networking and Communications (APWNC 2013 and APWNC 2015). He also organized the Future 5G Forum on Wireless Communications and Networking Big Data (FWCN 2016). He served as an Executive Co-Chairs of IEEE/CIC International Conference on Communications in China (ICCC), China, in 2019.

Zhuang Ling received the B.S. and Ph.D. degrees in College of Communication Engineering, Jilin University, Jilin, China, in 2016 and 2021, respectively. He was a visiting Ph.D. student with the Department of Electrical and Computer Engineering at University of Houston in 2020. Currently, he is a Postdoctoral Fellow in College of Communication Engineering, Jilin University, Jilin, China. His research interests include wireless body area network, backscatter communications, age of information, energy harvesting, and distributionally robust optimization.

Zhi Mao received the B.S. degree in communication engineering from the Changchun University of Science and Technology, Changchun, Jilin, China, in 2017. He received the Ph.D. degree from the College of Communication Engineering, Jilin University, Changchun, Jilin, China, in 2022. His current research interests include resource allocation and network optimization in 802.11 PHY protocol design.

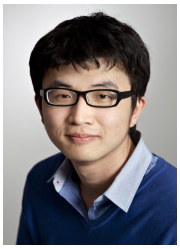

Zheng Chang received Ph.D degree from the University of Jyväskylä, Jyväskylä, Finland in 2013 . He has published over 140 papers in journals and conferences, and received best paper awards from IEEE TCGCC and APCC in 2017 and has been awarded as the 2018 IEEE Best Young Research Professional for EMEA and 2021 IEEE MMTC Outstanding Young Researcher. He has been served as symposium chair, publicity chair and workshop chair and also participated in organizing workshops and special sessions for many IEEE flagship conferences, such as Infocom, ICC and Globecom. He is an editor of Springer Wireless Networks, International Journal of Distributed Sensor Networks, and IEEE Wireless Communications Letters. He was the exemplary reviewer of IEEE Wireless Communication Letters in 2018. He also acts as a guest editor of IEEE Communications Magazine, IEEE Wireless Communications, IEEE Networks, IEEE Internet of Things Journal and IEEE Transactions on Industrial Informatics. His research interests include IoT, cloud/edge computing, security and privacy, vehicular networks, and green communications.

Cheng Li received his B. Eng. and M. Eng. degrees from Harbin Institute of Technology, Harbin, P. R. China, in 1992 and 1995, respectively, and his Ph.D. degree in Electrical and Computer Engineering from Memorial University, St. John's, Canada, in 2004.

He is currently a Full Professor and Head of the Department of Electrical and Computer Engineering of Memorial University, St. John's, Canada. His research interests include wireless communications and networking, communications signal processing, and mobile computing and computer networks. He has contributed 4 book chapters and over 350 research articles. He is an IEEE Communications Society Distinguished Lecturer for the 2021-22 term. He is an associate editor of the IEEE Transactions on Communications, the IEEE Internet-of-Things Journal, and the IEEE Network Magazine. He has served as the General Co-Chair of the ICNC'23, Q2SWinet'20, WINCOM'19, and AICON'19, and the TPC Co-Chair for the ICNC'20, ADHOCNETS'19, ACOSIS'19, WiCON'17, MSWiM'14, WiMob'11 and QBSC'10. He also served many times as a Technical Program Co-Chair for various technical symposia/tracks of international conferences, including the IEEE GLOBECOM, ICC, WCNC, and VTC. He served as the Chair of the IEEE Communications Society Ad Hoc and Sensor Networks Technical Committee (2018-19) and the Chair of the IEEE Newfoundland and Labrador Section (2012-13).

Dr. Li is the recipient of the Dean's Award for Research Excellence at Memorial University in 2021, the recipient of the Technical Achievement Award of the IEEE Communications Society Communications Software Technical Committee in 2018, and the recipient of several Best Paper Awards at international conferences, including the IEEE Globecom'2017 and ICC'2010. He is a registered Professional Engineer (P.Eng.) in Canada and is a Senior Member of the IEEE and a member of the IEEE Communication Society, Computer Society, Vehicular Technology Society, and Ocean Engineering Society.